Efficient and specific DNA-targeting using single-stranded LNA/MOE mixmers and chimeric Invader:XenoRNA probes

Michaela E. Everly[a] and Patrick J. Hrdlicka[a]

[a] Department of Chemistry, University of Idaho, Moscow, Idaho 83844-2343, USA

E-mail: hrdlicka@uidaho.edu

Electronic Supplementary Information

EXPERIMENTAL SECTION

Synthesis and purification of probe strands. All XRNAs were purchased from a commercial vendor and used as received (for ESI-MS spectra and capillary electrophoresis electropherograms, see Table S6 and Figs. S10–S16). The **INVu**, **INVd**, and **LNA1** strands were available from prior studies (ESI-MS and HPLC chromatograms reported therein).[S1,S2]

Thermal denaturation experiments, determination of thermodynamic parameters, and UV-Vis experiments. Concentrations of XRNA strands were estimated using the following RNA extinction coefficients (OD$_{260}$/µmol): G (13.7), A (15.4), T (10.0), and C (7.4) (for fully modified O2'-Me and 2'-F strands) or $^{5\text{-Me}}$C (9.0) (for fully modified MOE, LNA/MOE mixmers, and **LNA1**). Concentrations of **INVu**, **INVd**, and DNA strands were estimated using the following DNA extinction coefficients (OD$_{260}$/µmol): G (12.01), A (15.20), T (8.40), C (7.05), and pyrene (22.4)[S3]. T_ms of duplexes (1.0 µM final concentration of each strand) were determined on a Cary 100 UV/VIS spectrophotometer equipped with a 12-cell Peltier temperature controller and measured as the maximum of the first derivative of thermal denaturation curves (A_{260} vs. T) recorded in medium salt buffer unless otherwise specified ([Na$^+$] = 110 mM, [Cl$^-$] = 100 mM, pH 7.0 (NaH$_2$PO$_4$/Na$_2$HPO$_4$), [EDTA] = 0.2 mM). Strands were mixed in quartz optical cells with a path length of 1.0 cm and annealed by heating to 90 °C (2 min) followed by cooling to the starting temperature of the experiment. The temperature of the denaturation experiments ranged from at least 15 °C below the T_m to at least 15 °C above the T_m (although not below 10 °C nor above 95 °C). A temperature ramp of 0.5 °C/min was used in all experiments. Reported T_ms are averages of at least two experiments within ± 1.0 °C. T_ms of some XRNA-containing duplexes were

determined from differential thermal denaturation curves to eliminate the impact of XRNA-based secondary structure denaturation (indicated in table footnotes). Thermodynamic parameters associated with duplex formation were determined through baseline fitting of thermal denaturation curves (van't Hoff method) using the software provided with the UV-Vis spectrophotometer. Bimolecular reactions, two-state melting behavior, and constant heat capacity are assumed.[S4] Denaturation curves were fitted at least three times to minimize errors arising from baseline choice.

Absorption spectra (range 200–600 nm) were recorded at 10 °C using the T_m samples (i.e., each strand used at 1.0 µM in T_m buffer) and instrumentation as in the thermal denaturation experiments.

dsDNA-invasion experiments. The dsDNA-invasion experiments were performed following an established protocol.[S5] Briefly, DNA hairpins were obtained from commercial sources and used as received. A recombinant terminal transferase was used to incorporate 11-digoxigenin-ddUTP at the 3'-end of the hairpins. The reaction was quenched through addition of 0.05 M EDTA, and the mixture diluted to a working concentration and used without further processing.

Solutions of chimeric, Invader, and XRNA probes (concentrations as specified) were incubated with the corresponding digoxigenin (DIG)-labeled DNA hairpin (final concentration 50 nM) in HEPES buffer (50 mM HEPES, 100 mM NaCl, 5 mM MgCl$_2$, pH 7.2, 10% sucrose, 1.44 mM spermine tetrahydrochloride) at 37 °C for 17 h. Following incubation, loading dye (6X) was added and the mixtures were loaded onto 20% non-denaturing TBE-PAGE slabs (45 mM tris-borate, 1

mM EDTA; acrylamide:bisacrylamide (19:1)). Incubation mixtures were resolved via electrophoresis, which was performed using constant voltage (~70 V) at ~4 °C for ~4 h.

Bands were subsequently blotted onto positively charged nylon membranes (~100 V, ~30 min, ~4 °C) and cross-linked through exposure to UV light (254 nm, 5 × 15 W bulbs, 5 min). The membranes were then incubated with Anti-Digoxigenin-Alkaline Phosphatase Fab fragments and transferred to a hybridization jacket. Membranes were then incubated with the chemiluminescence substrate (CDP-Star) for 10 min at 37 °C whilst being shielded from light. Chemiluminescence of the formed product was captured and quantified (as the intensity ratios between the bands corresponding to the recognition complexes and unbound hairpin) using the C-DiGit® Blot Scanner (LI-COR) and accompanying software (Image Studio). An average of at least three independent experiments for the fixed-dose and dose-response invasion assays, and at least two independent experiments for binding specificity assays, is reported along with standard deviations (±). The electrophoretograms shown are in some instances composite images of lanes from different runs (indicated in the respective figure legends).

C_{50} values were determined using a custom R script that automates non-linear curve fitting and calculation of C_{50} values. Additional custom R scripts were used to plot and visualize the data presented herein. All R scripts are available through version-controlled public repositories.[S6,S7]

SUPPORTING DISCUSSIONS AND FIGURES

Definition of zipper nomenclature. The relative arrangement between two 2′-*O*-(pyren-1-yl)methyl-RNA monomers (and more generally, two intercalator-functionalized nucleotide monomers) on opposing strands in an Invader probe is described by the following nomenclature: the number *n* is the distance (measured in number of base pairs) between the two monomers and has a positive value if a monomer is shifted toward the 5'-side of its strand relative to the monomer on the opposite strand, and has a negative value a monomer is shifted toward the 3'-side of its strand relative to the monomer on the opposite strand.

Additional discussion of the "nearest neighbor exclusion principle". According to the nearest neighbor exclusion principle (NNEP), a local intercalator density exceeding one per two base pairs in a DNA duplex is unfavorable due to reduced base pair stacking and excessive unwinding of the duplex.[S8] This is due to limitations in local helix expandability (each intercalation event expands the duplex by ~3.4 Å) and because the stabilizing stacking interactions between neighboring base pairs and a first intercalating moiety become perturbed upon intercalation of a second intercalator.[S8-S11] Every hotpot in an Invader probe features two intercalators per two base pairs; the probe duplex and therefore becomes partially unwound and labile (i.e., the NNEP is violated).[S12,S13] Conversely, duplex formation between individual Invader strands and cDNA results in strongly stabilizing stacking interactions between the intercalator and flanking base pairs (i.e., local intercalator density is at the limit of the NNEP).
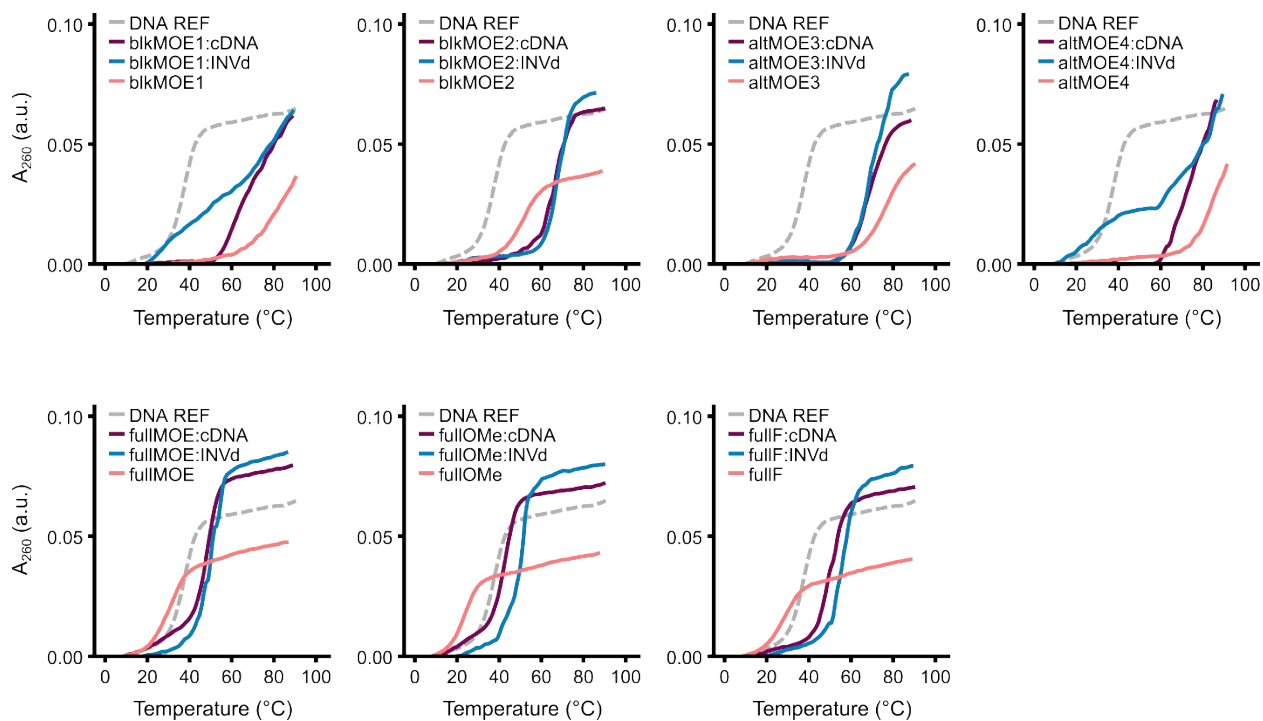
Figure S1. Representative thermal denaturation curves for XRNA:cDNA duplexes, chimeric probe duplexes, and single-stranded XRNAs. "DNA REF" is the corresponding unmodified DNA reference duplex. For sequences of strands and experimental conditions, see Table 1.

Additional discussion concerning thermal denaturation profiles of chimeric probes. Differential thermal denaturation curves were constructed to eliminate potential contributions of XRNA-only secondary structures to the observed denaturation profiles of the chimeric Invader:XRNA probes (Fig. S2). Thus, XRNA-only denaturation profiles were subtracted from the corresponding chimeric probe profiles or XRNA:cDNA profiles using the *Maths* function in the Cary WinUV Thermal Application. This allowed for a more reliable determination of T_m and TA values (Table 1).

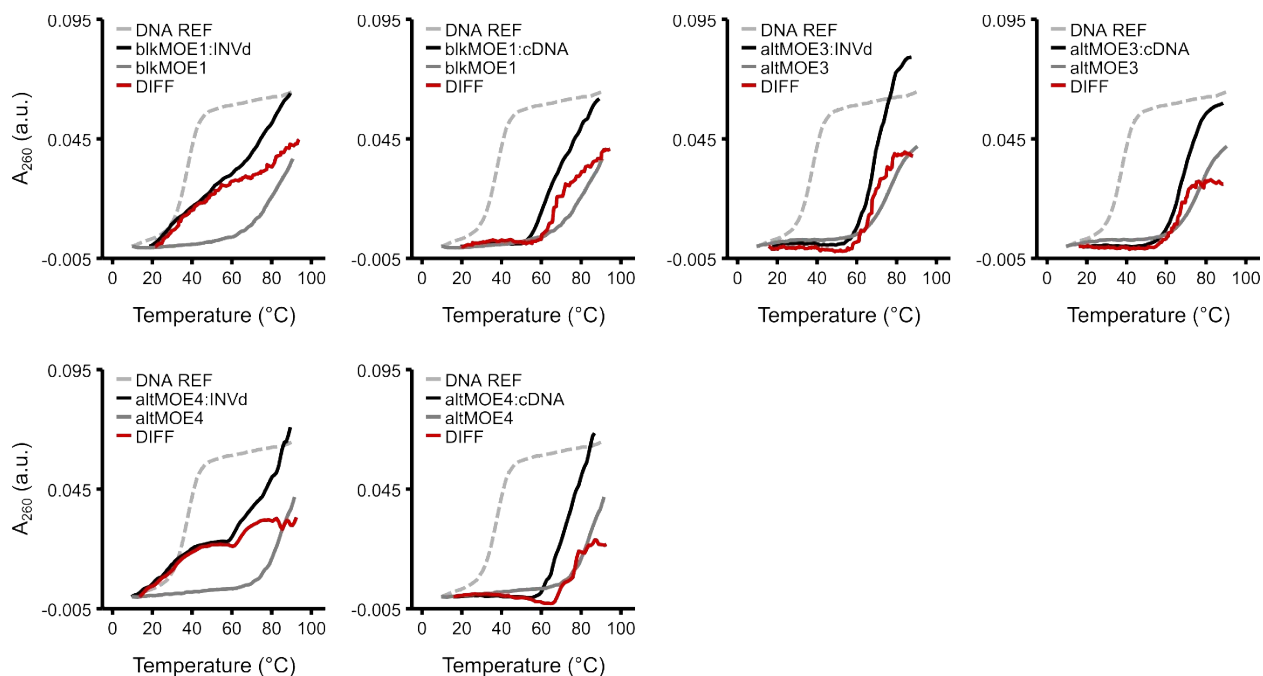**Figure S2.** Representative differential thermal denaturation curves of duplexes between XRNAs and **INVd** or cDNA. Curves were obtained by subtracting the T_m profile of the single-stranded XRNA from the profiles of the corresponding double-stranded chimeric probe or XRNA:cDNA profiles. "DNA REF" is the corresponding unmodified DNA reference duplex. See Table 1 for experimental conditions.
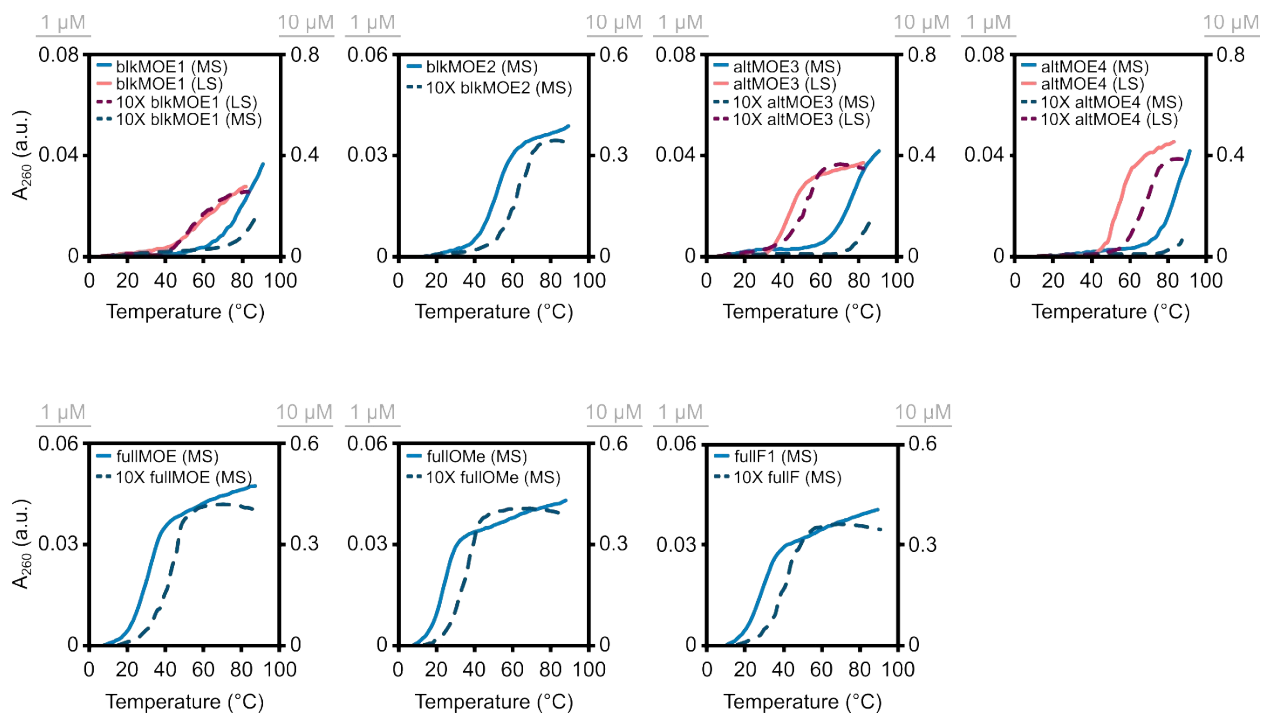
Figure S3. Representative thermal denaturation curves for single-stranded XRNAs at 1 μM and 10 μM concentrations in medium salt (MS; $[Na^+]$ = 110 mM, $[Cl^-]$ = 100 mM, pH 7.0 (NaH_2PO_4/Na_2HPO_4), [EDTA] = 0.2 mM) or low salt (LS; $[Na^+]$ = 10 mM, pH 7.0 ($NaH_2PO_4/Na2HPO_4$), [EDTA] = 0.2 mM) phosphate buffers. Left and right Y-axes depict A_{260} values for probes used at 1 μM and 10 μM concentration, respectively.

Table S1. T_ms of single-stranded XRNAs at 1 µM and 10 µM probe concentrations. [a]

Name	Probe	T_m [ΔT_m] (°C)	
		1 µM	10 µM
blkMOE1	5'-GGTATATATAGGC-3'	~58.0 [b,c]	~58.0 [b,c]
blkMOE2	5'-GGTATATATAGGC-3'	53.0	60.5
altMOE3	5'-GGTATATATAGGC-3'	46.0 [b]	52.5 [b]
altMOE4	5'-GGTATATATAGGC-3'	54.5 [b]	71.0 [b]
fullMOE	5'-GGTATATATAGGC-3'	34.5	41.5
fullOMe	5'-GGUAUAUAUAGGC-3'	24.0	35.0
fullF	5'-GGUAUAUAUAGGC-3'	28.0	40.0

[a] LNA, MOE, O2'-Me, and 2'-F modifications are represented as dark purple, peach, light purple, and green circles, respectively. Structures of modifications are shown in Fig. 1. Thermal denaturation curves (Fig. S3) were recorded as described in Table 1 except as pointed out in footnote "b" where relevant. [b] T_ms were determined in low salt phosphate buffer ([Na^+] = 10 mM, pH 7.0 (NaH_2PO_4/Na_2HPO_4), [EDTA] = 0.2 mM) to reduce stability and move high-melting transitions into view. [c] Broad transition observed.

Available thermodynamic driving force for recognition of complementary dsDNA targets. The available free energy for recognition of complementary dsDNA targets at 310 K by double-stranded probes can be estimated using changes in Gibbs free energy in an equivalent manner as with the T_m-based TA term, i.e., ΔG_{rec}^{310} = ΔG^{310} (upper strand vs. cDNA) + ΔG^{310} (lower strand vs. cDNA) − ΔG^{310} (probe duplex) − ΔG^{310} (dsDNA) (Table S2). More negative ΔG_{rec}^{310} values are indicative of a more favorable driving force for dsDNA target recognition. For single-stranded probes, the term reduces to ΔG_{rec}^{310} = ΔG^{310} (probe vs. cDNA) − ΔG^{310} (dsDNA), which is simply the $\Delta\Delta G^{310}$ value for a probe:cDNA duplex.

Overall, the results point to similar conclusions as the T_m-based terms. Briefly, chimeric Invader:XRNA probes are more stable than the corresponding conventional Invader probe ($\Delta\Delta G$ = −56 to −18 kJ mol^{-1} vs. −11 kJ mol^{-1}, respectively), with the chimeric Invader:LNA/MOE probes, and **blkMOE2:INVd** especially, being particularly stable (Table S2). Duplexes between LNA/MOE mixmers and cDNA are of a similar stability as duplexes between individual Invader strands and cDNA ($\Delta\Delta G$ = −36 to −35 kJ mol^{-1}), whereas the corresponding duplexes between the other XRNAs and cDNA are less stable ($\Delta\Delta G$ = −20 to −9 kJ mol^{-1}). As a result, the driving force for dsDNA-recognition is lower for the chimeric probes than for the Invader probe (ΔG_{rec}^{310} = −36 to −15 kJ mol^{-1} vs. −62 kJ mol^{-1}, respectively).

Comparison of ΔG_{rec}^{310} values suggests that the available thermodynamic driving force for dsDNA-invasion is similar for the chimeric probes entailing the fully modified MOE, O2'-Me, and

2'-F strands, **altMOE3:INVd**, and the single-stranded LNA/MOE mixmers (ΔG_{rec}^{310} = −36 to −27 kJ mol^{-1}), but less favorable for **blkMOE2:INVd** and the fully modified MOE, O2'-Me, and 2'-F strands (ΔG_{rec}^{310} = −20 to −9 kJ mol^{-1}). It should be noted that the calculated ΔG_{rec}^{310} values do not account for potential secondary structure formation of the single-stranded probes. Additionally, we caution against overinterpreting the ΔG_{rec}^{310} values as the accuracy of the underlying Gibbs free energy values is likely impacted by the irregular nature of the denaturation profiles.

Table S2. Change in Gibbs free energy at 310 K (ΔG^{310}) upon formation of chimeric probe duplexes, and duplexes between individual probe strands and cDNA, and the available free energy for recognition of complementary dsDNA by double-stranded probes (ΔG^{310}_{rec}). [a]

Name	Probe	ΔG^{310} [$\Delta\Delta G^{310}$] (kJ mol^{-1})			ΔG^{310}_{rec}
		Probe Duplex	Upper strand vs. cDNA	Lower strand vs. cDNA	
blkMOE1 INVd	5'-GGTATATATAGGC-3' 3'-CCAUAUAUAUCCG-5'	n.d.	n.d.	−78 [−36]	n.d.
blkMOE2 INVd	5'-GGTATATATAGGC-3' 3'-CCAUAUAUAUCCG-5'	−98 [−56]	−77 [−35]	−78 [−36]	−15
altMOE3 INVd	5'-GGTATATATAGGC-3' 3'-CCAUAUAUAUCCG-5'	−81 [−39]	−77 [−35]	−78 [−36]	−32
altMOE4 INVd	5'-GGTATATATAGGC-3' 3'-CCAUAUAUAUCCG-5'	n.d.	−78 [−36]	−78 [−36]	n.d.
fullMOE INVd	5'-GGTATATATAGGC-3' 3'-CCAUAUAUAUCCG-5'	−61 [−19]	−61 [−19]	−78 [−36]	−36
fullOMe INVd	5'-GGUAUAUAUAGGC-3' 3'-CCAUAUAUAUCCG-5'	−60 [−18]	−51 [−9]	−78 [−36]	−27
fullF INVd	5'-GGUAUAUAUAGGC-3' 3'-CCAUAUAUAUCCG-5'	−70 [−28]	−62 [−20]	−78 [−36]	−28
INVu INVd	5'-GGUAUAUAUAGGC-3' 3'-CCAUAUAUAUCCG-5'	−53 [−11]	−78 [−36]	−78 [−37]	−62

[a] $\Delta\Delta G^{310}$ is determined relative to the corresponding unmodified DNA duplex (ΔG^{310} = −42 kJ mol^{-1}). For a definition of ΔG^{310}_{rec}, see above discussion n.d. = not determined due to unclear baseline. For experimental conditions, see Table 1. Data for entries in "lower strand vs. cDNA" column and **INVu:INVd** are from Ref. S1.

Discussion on UV-Vis characterizations of the oligonucleotides studied herein. To gain insight into the placement of the pyrene moieties in the different duplexes, UV-Vis spectra were recorded for **INVd** and the corresponding duplexes with complementary XRNA, Invader, or cDNA strands. Pyrene intercalation upon duplex formation is expected to result in bathochromic shifts of the pyrene absorption bands relative to the individual Invader strand, whereas hypsochromic shifts are expected if duplex formation reduces electronic interactions between pyrenes and nucleobases.[S14] **INVd** displays pyrene absorption maxima in the 333–334 nm and 348–350 nm range (Fig. S4 and Table S3). A prominent hypsochromic shift is observed upon hybridization with **INVu**, whereas a bathochromic shift is observed upon hybridization with cDNA (Fig. S4 and Table S3). Surprisingly, bathochromic shifts are also observed upon hybridization with the XRNAs, which suggests that the XRNA modifications do not significantly deter pyrene intercalation, consistent with the unexpectedly high stability of the chimeric probes.
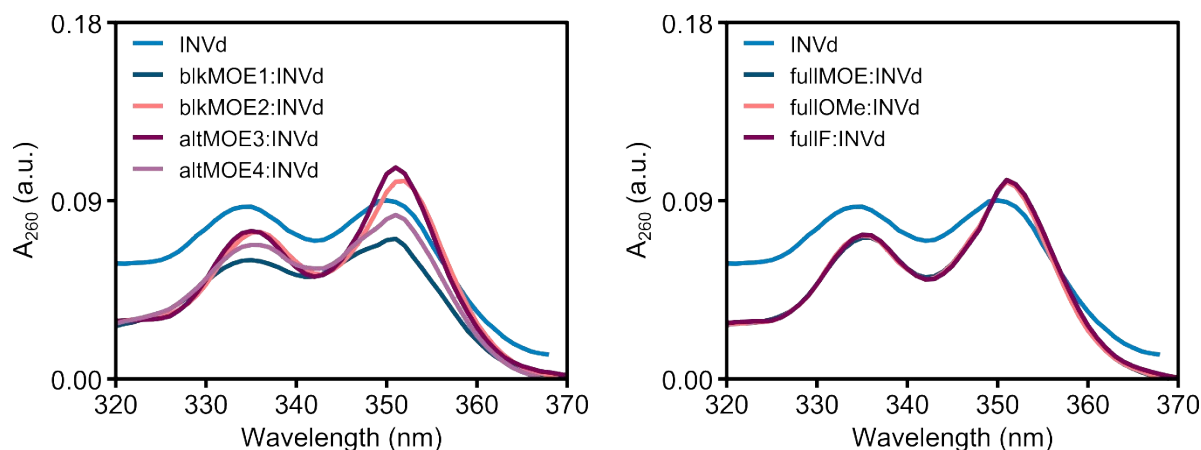
Figure S4. Representative UV-Vis absorption spectra for single-stranded **INVd** and the corresponding duplexes with complementary XRNAs. Spectra were recorded at 10 °C in medium salt buffer using quartz optical cells with a 1.0 cm path length. The spectrum for **INVd** was previously reported in Refs. S2 and S15.

Table S3. Absorption maxima in the 340–365 nm region observed for single-stranded **INVd** and the corresponding duplexes with complementary **INVu**, XRNAs, LNA, or DNA. [a]

Probe	λ_{max} (nm) [$\Delta\lambda_{max}$]
INVd	349 [b]
+INVu	346 [−3] [b]
+blkMOE1	351 [+2]
+blkMOE2	352 [+3]
+altMOE3	351 [+2]
+altMOE4	351 [+2]
+fullMOE	351 [+2]
+fullOMe	351 [+2]
+fullF	352 [+3]
+LNA1	350 [+1] [b]
+cDNA	352 [+3] [b]

[a] $\Delta\lambda_{max}$ is calculated relative to single-stranded **INVd**. Spectra were recorded at 10 °C in medium salt T_m buffer using quartz optical cells with a 1.0 cm path length. [b] Data previously reported.[S2] See Fig. S4 for corresponding UV-Vis absorption spectra.

Table S4. Extent of **DH1** invasion when using chimeric Invader:XRNA and single-stranded XRNA probes at 5-fold molar excess. [a]

Probe	Invasion at 5x (%)	Probe	Invasion at 5x (%)
blkMOE1:INVd	97 ± 1	**fullMOE:INVd**	34 ± 10
blkMOE2:INVd	41 ± 11	**fullOMe:INVd**	35 ± 5
altMOE3:INVd	88 ± 4	**fullF:INVd**	64 ± 2
altMOE4:INVd	82 ± 5	**fullMOE**	13 ± 4
blkMOE1	94 ± 5	**fullOMe**	<1 ± 1
blkMOE2	100 ± 0	**fullF**	13 ± 5
altMOE3	93 ± 4		
altMOE4	45 ± 20		

[a] See Fig. 3 for representative electrophoretograms and assay details. "Invasion at 5x" = percent of **DH1** invasion when using 5-fold molar probe excess; "±" = standard deviation from at least three trials.
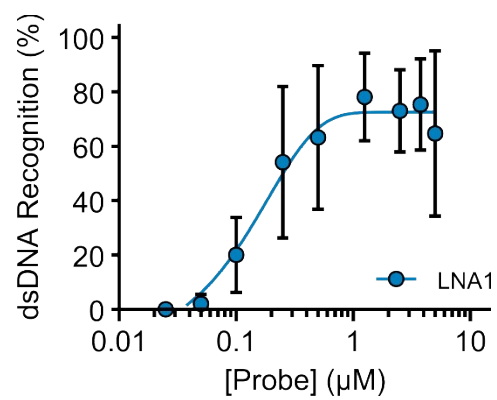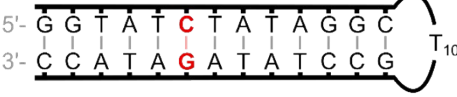
Figure S5. Updated dose-response curve for single-stranded **LNA1**. For experimental conditions, see Fig. 3.

Table S5. Sequences and T_ms of DNA hairpins used in this study. [a]

Hairpin	Sequence	T_m (°C)
DH1	5'- G G T A T A T A T A G G C / 3'- C C A T A T A T A T C C G — T_{10}	58.5
DH2	5'- G G T A T **T** T A T A G G C / 3'- C C A T A **A** A T A T C C G — T_{10}	60.5
DH3	5'- G G T A T **G** T A T A G G C / 3'- C C A T A **C** A T A T C C G — T_{10}	63.5
DH4	5'- G G T A T **C** T A T A G G C / 3'- C C A T A **G** A T A T C C G — T_{10}	63.0
DH5	5'- G G T A T A T A **A** A G G C / 3'- C C A T A T A T **T** T C C G — T_{10}	60.0
DH6	5'- G G T A T A T A **G** A G G C / 3'- C C A T A T A T **C** T C C G — T_{10}	62.5
DH7	5'- G G T A T A T A **C** A G G C / 3'- C C A T A T A T **G** T C C G — T_{10}	62.5

[a] For experimental conditions, see Table 1. T_m values have been previously reported in Ref. S16 and are included here for convenience.
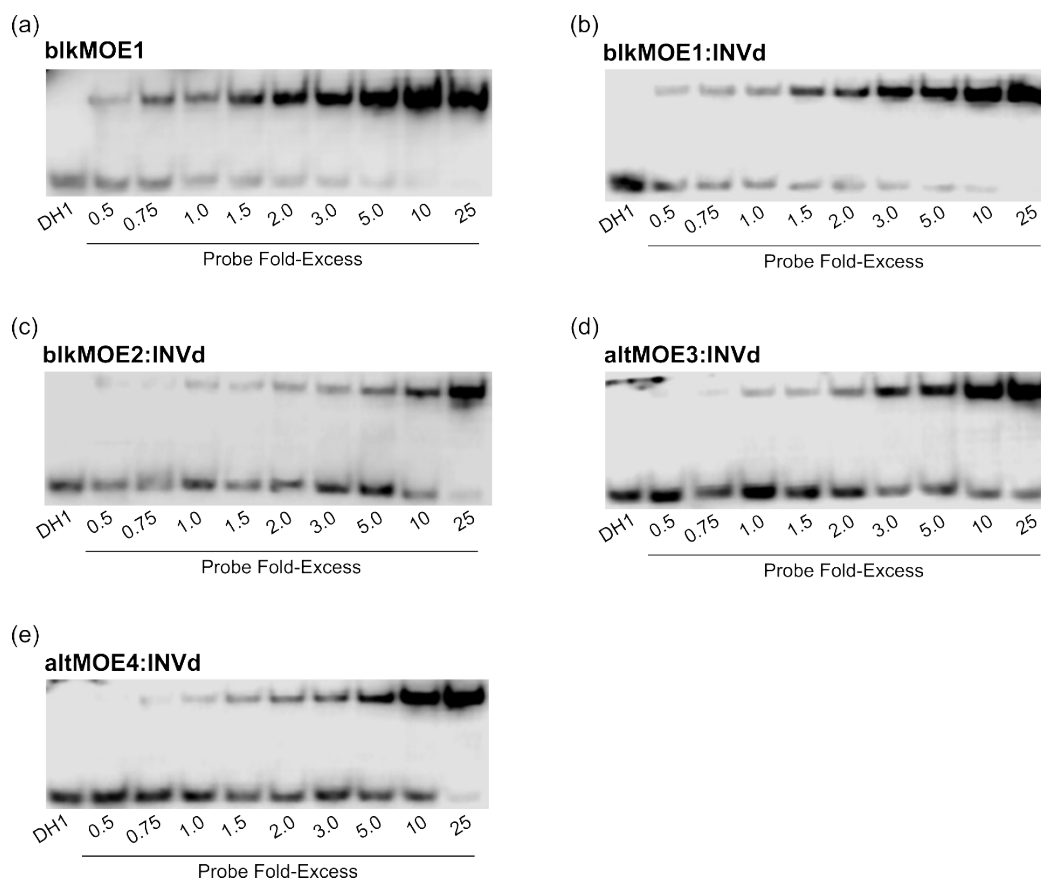
Figure S6. Representative electrophoretograms for dose-response experiments in which **DH1** (50 nM) was incubated alone (left lanes) or with variable molar fold-excess of the indicated probes. Conditions are otherwise as described in Fig. 3.
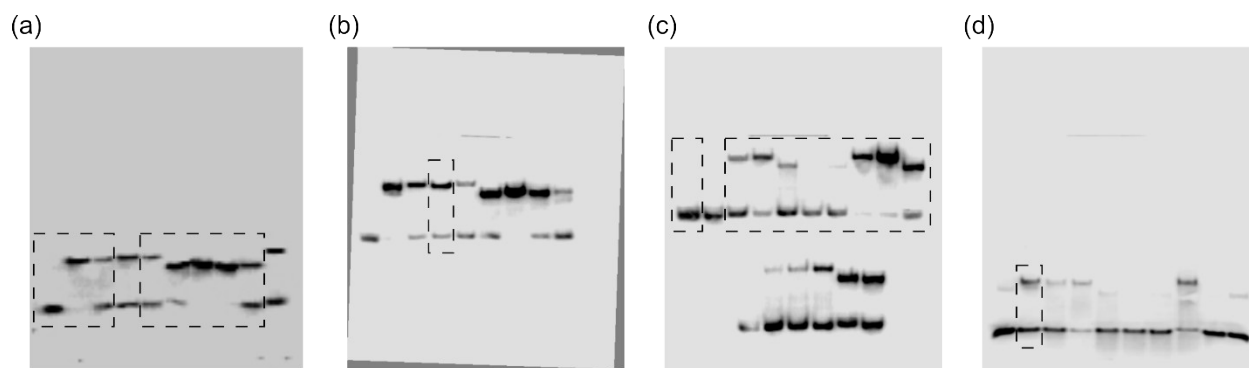
Figure S7. Uncropped images of gel blots for electrophoretograms in (a, b) Fig. 3c and (c, d) Fig. 3b. The full images were processed using Image Studio Digits Ver 5.2 software as follows: first, an image was subjected to the "Noise Removal" operation (1x). Second, contrast was adjusted such that background signals were reduced but all bands remained visible. Dashed boxes indicate the specified lanes used to construct the respective electrophoretogram. All bands located below the dashed box in (b) are from a separate gel blot that was simultaneously imaged with the specified blot. The faint horizontal line above the blots is from the surface of the scanner and not the blot. For full details, see the comprehensive protocol in Ref. S5.
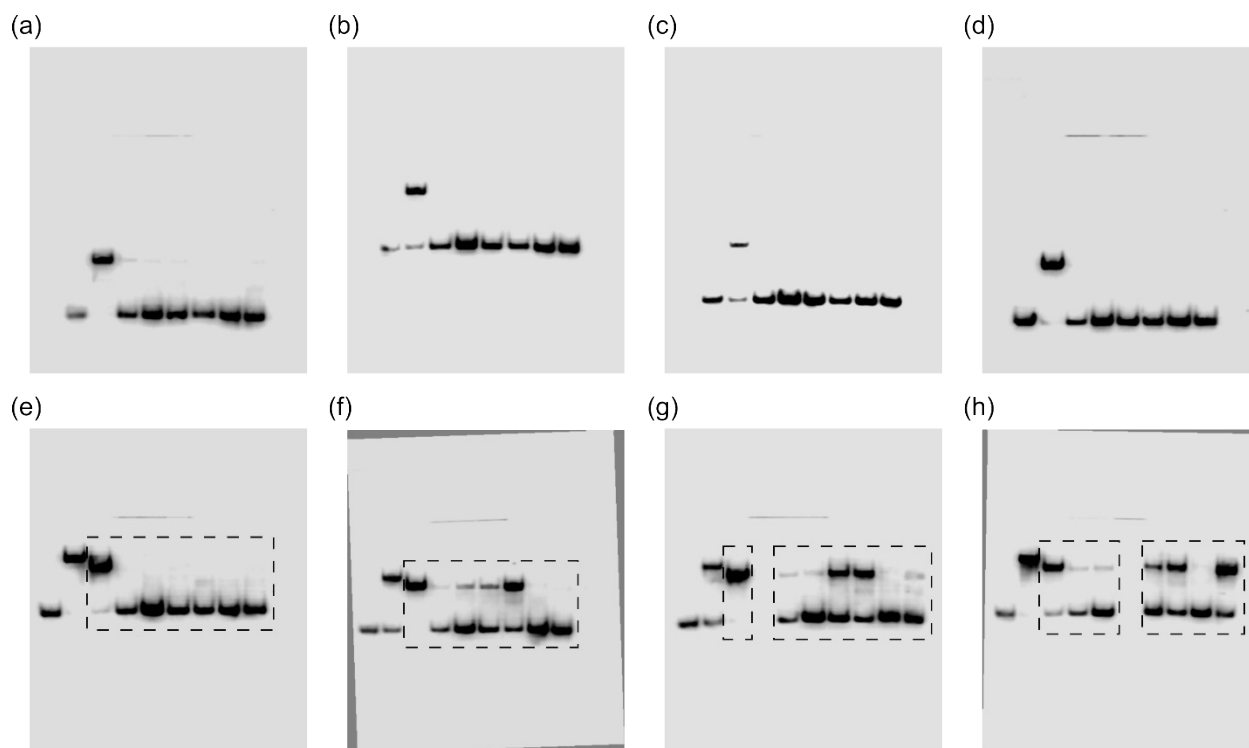
Figure S8. Uncropped images of gel blots for electrophoretograms in Fig. 4, i.e., specificity experiments for (a) blkMOE1:INVd, (b) blkMOE2:INVd, (c) altMOE3:INVd, (d) altMOE4:INVd, (e) blkMOE1, (f) blkMOE2, (g) altMOE3, and (h) altMOE4. Images were processed as described in Fig. S7. Dashed boxes indicate the specified lanes used to construct the respective electrophoretogram. The faint horizontal line above some of the blots is from the surface of the scanner and not the blot.
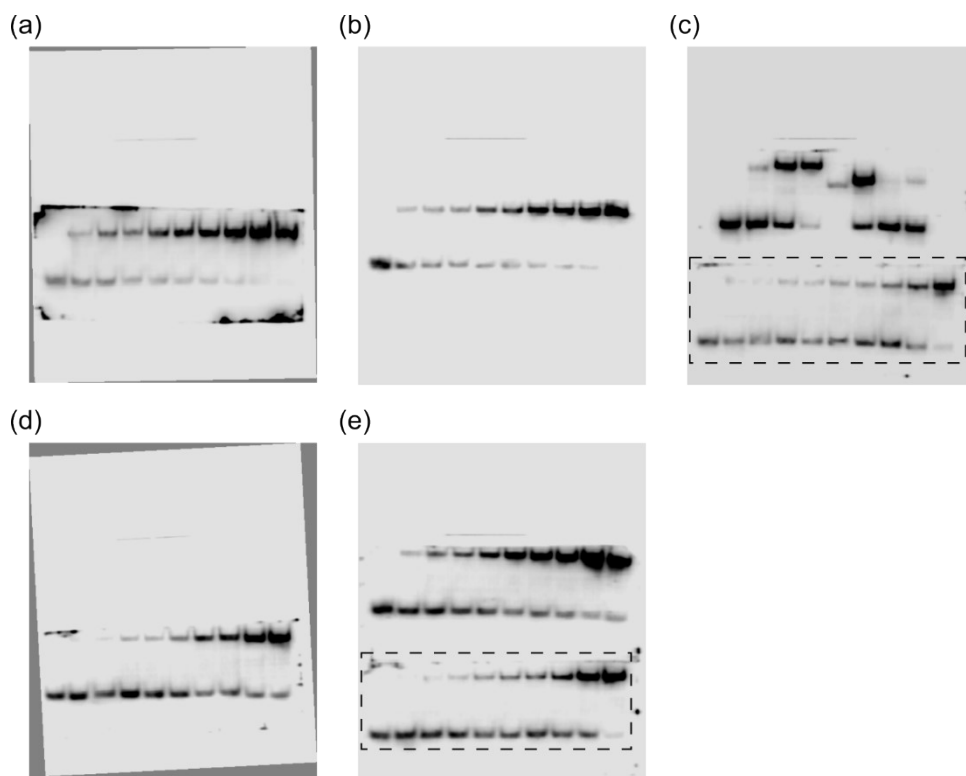
Figure S9. Uncropped images of gel blots for electrophoretograms in Fig. S6, i.e., dose-response experiments for (a) blkMOE1, (b) blkMOE1:INVd, (c) blkMOE2:INVd, (d) altMOE3:INVd, and (e) altMOE4:INVd. Images were processed as described in Fig. S7. Dashed boxes indicate the specified lanes used to construct the respective electrophoretogram. All bands located above the dashed box in (c) and (e) are from a separate gel blot that was simultaneously imaged with the specified blot. The faint horizontal line above the blots is from the surface of the scanner and not the blot.

Table S6. ESI-MS data for the single-stranded XRNAs. [a]

XRNA	Calculated m/z (M-H)⁻	Observed m/z (M-H)⁻
blkMOE1	4714.3	4714.3
blkMOE2	4668.2	4668.6
altMOE3	4714.3	4714.5
altMOE4	4668.2	4668.6
fullMOE	4990.7	4991.0
fullOMe	4347.9	4348.3
fullF	4191.4	4192.0

[a] See Table S1 for sequences.
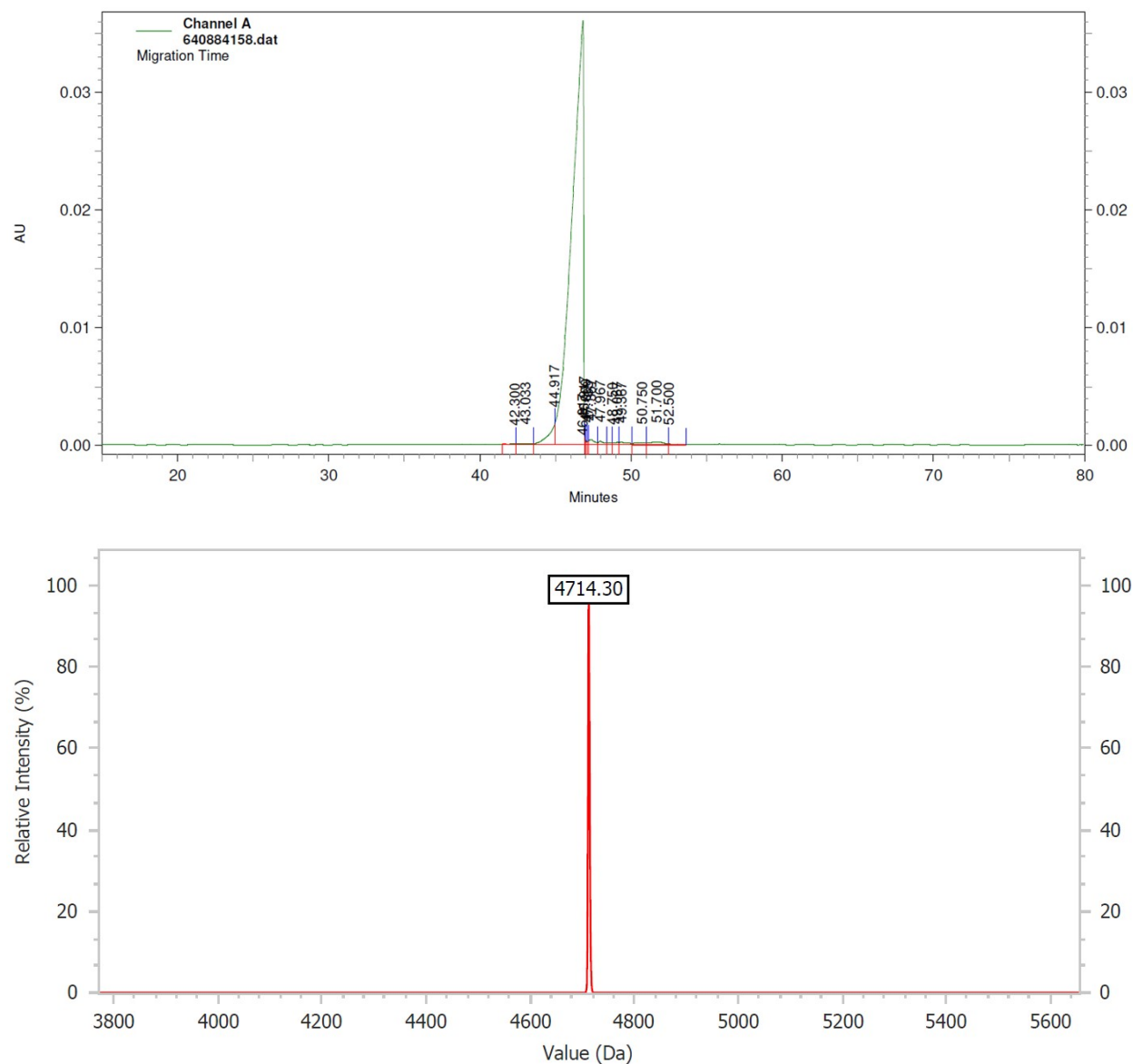
Figure S10. Capillary electrophoresis electropherogram (top) and ESI-MS spectrum (bottom) for **blkMOE1**. Data provided by IDT.
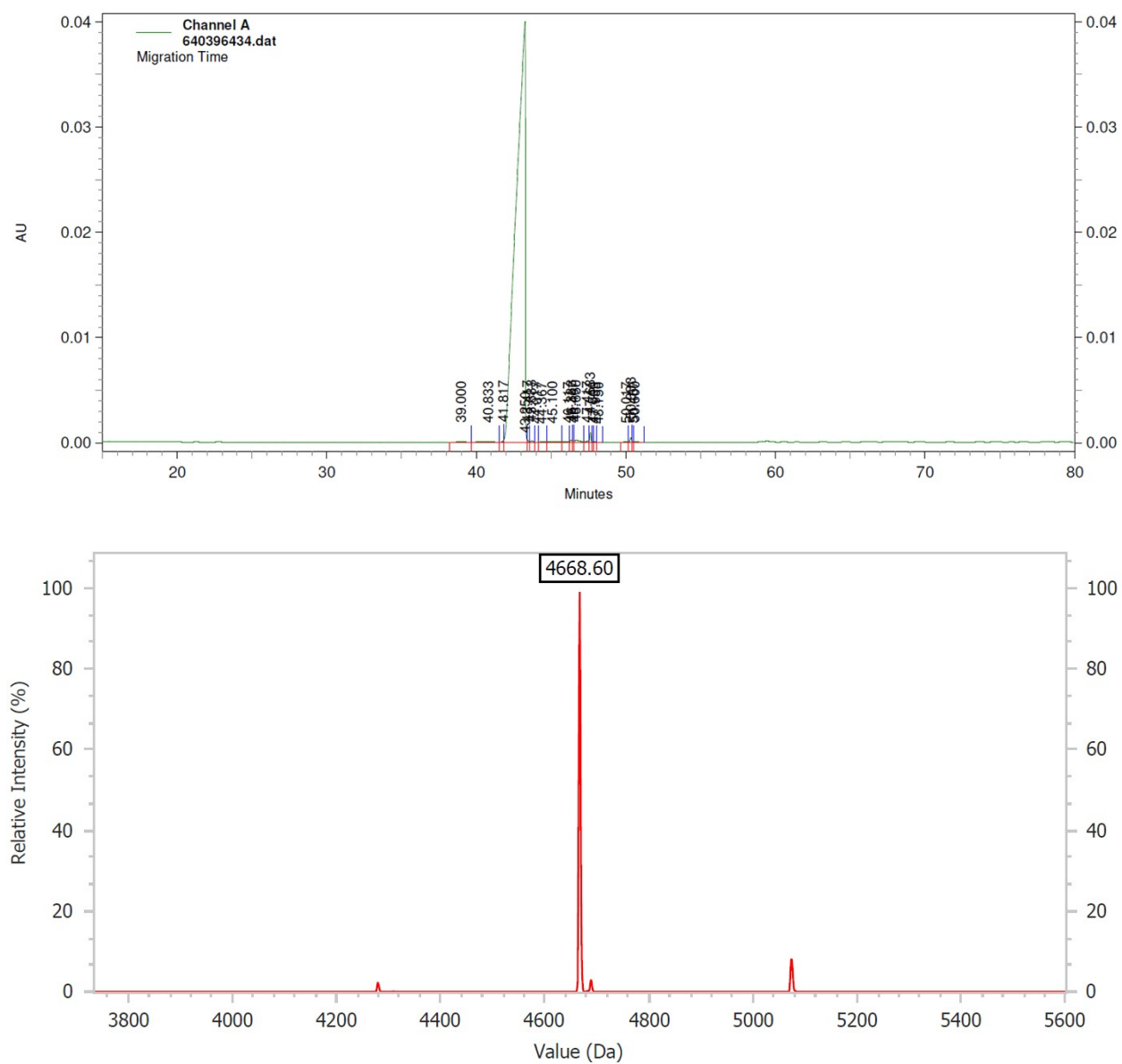
Figure S11. Capillary electrophoresis electropherogram (top) and ESI-MS spectrum (bottom) for **blkMOE2**. Data provided by IDT.
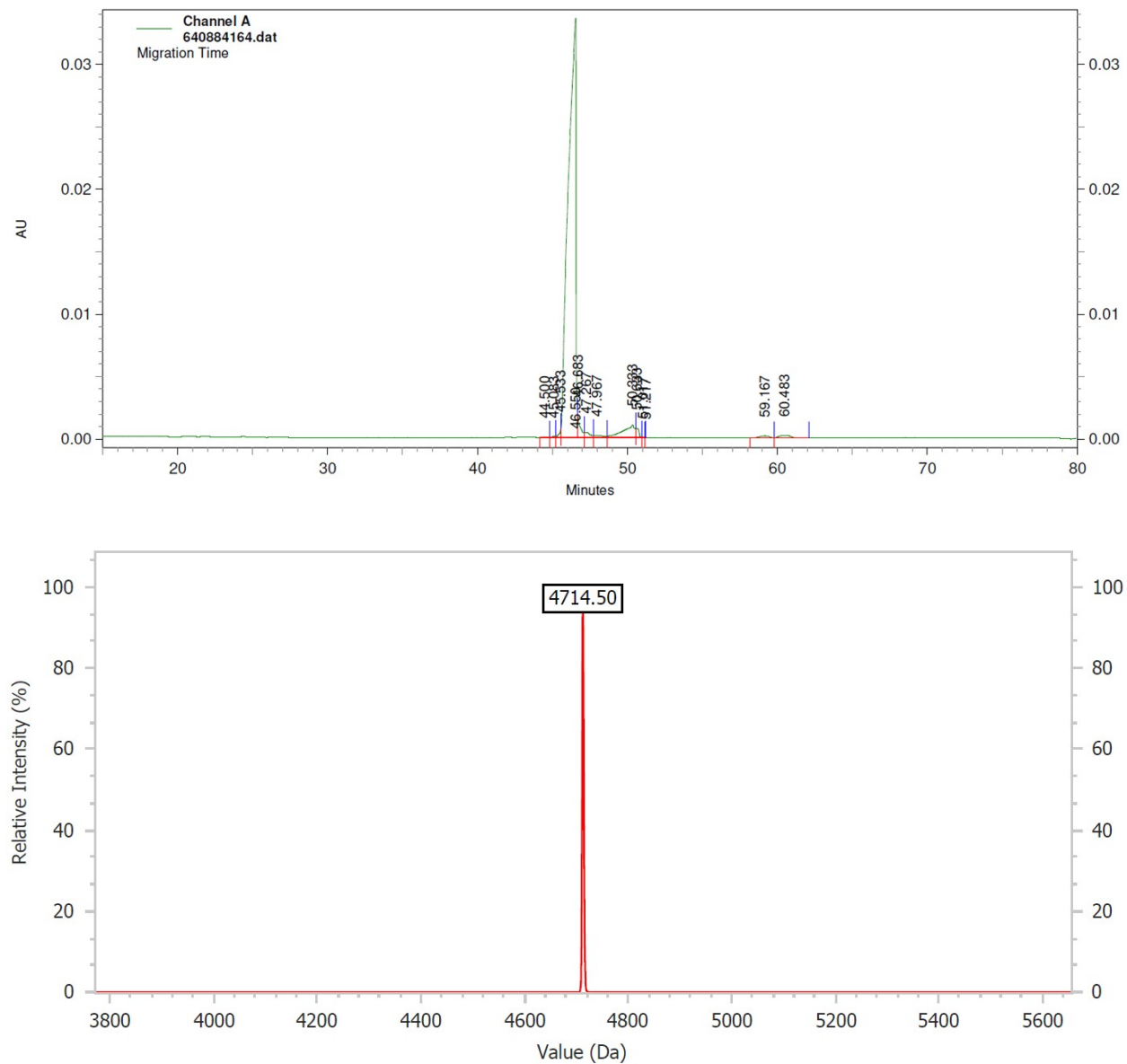
Figure S12. Capillary electrophoresis electropherogram (top) and ESI-MS spectrum (bottom) for **altMOE3**. Data provided by IDT.
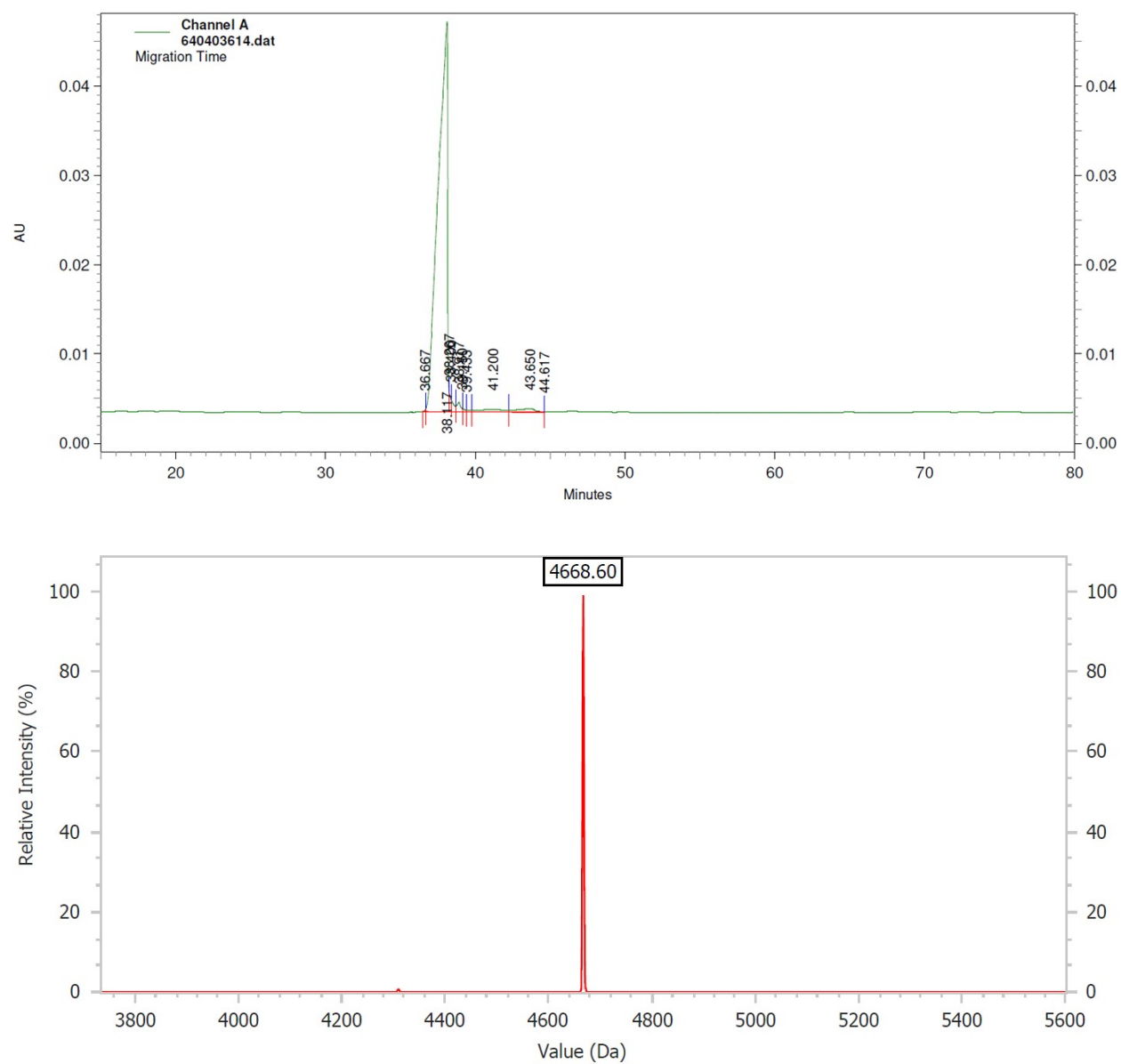
Figure S13. Capillary electrophoresis electropherogram (top) and ESI-MS spectrum (bottom) for **altMOE4**. Data provided by IDT.
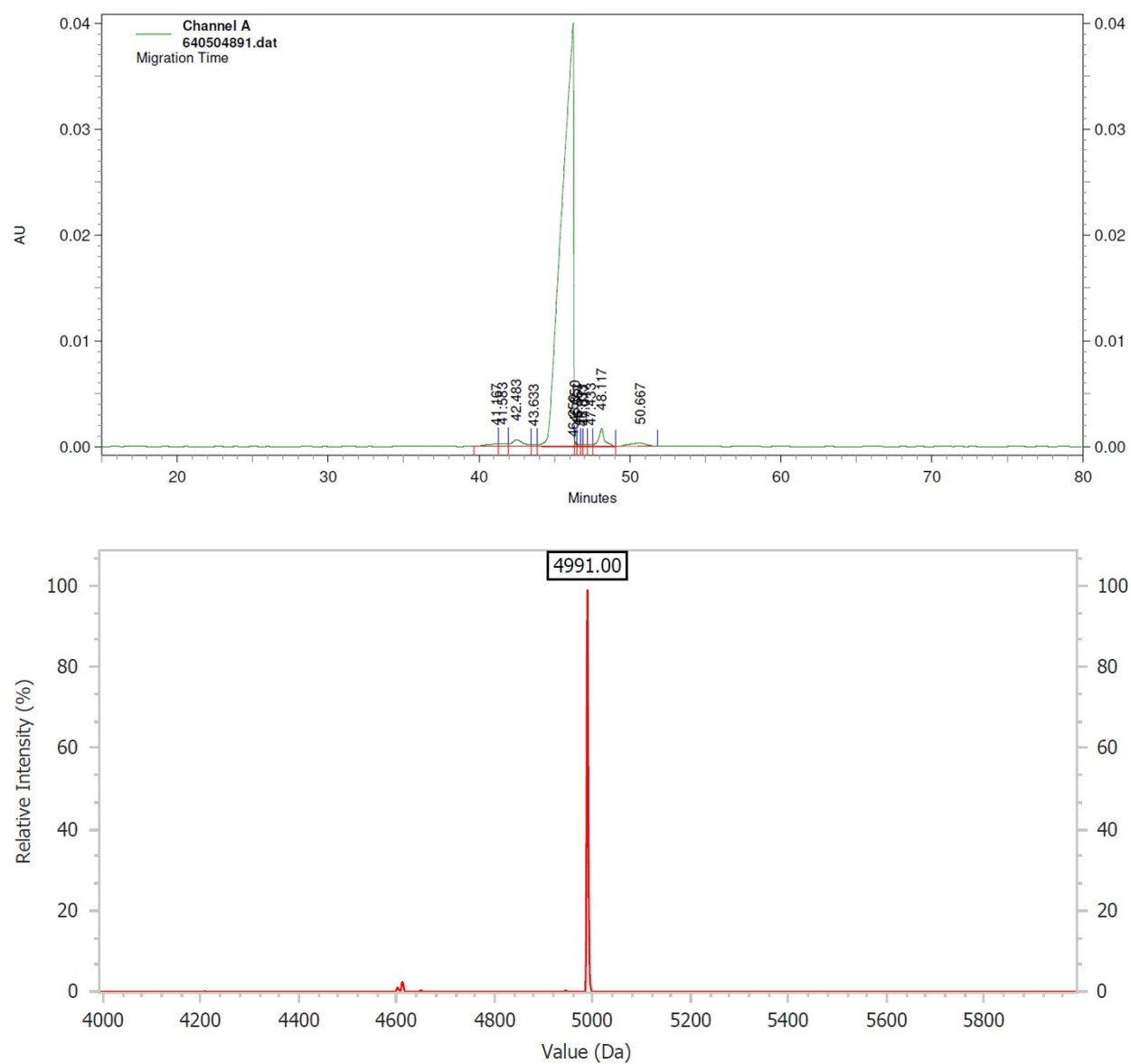
Figure S14. Capillary electrophoresis electropherogram (top) and ESI-MS spectrum (bottom) for **fullMOE**. Data provided by IDT.
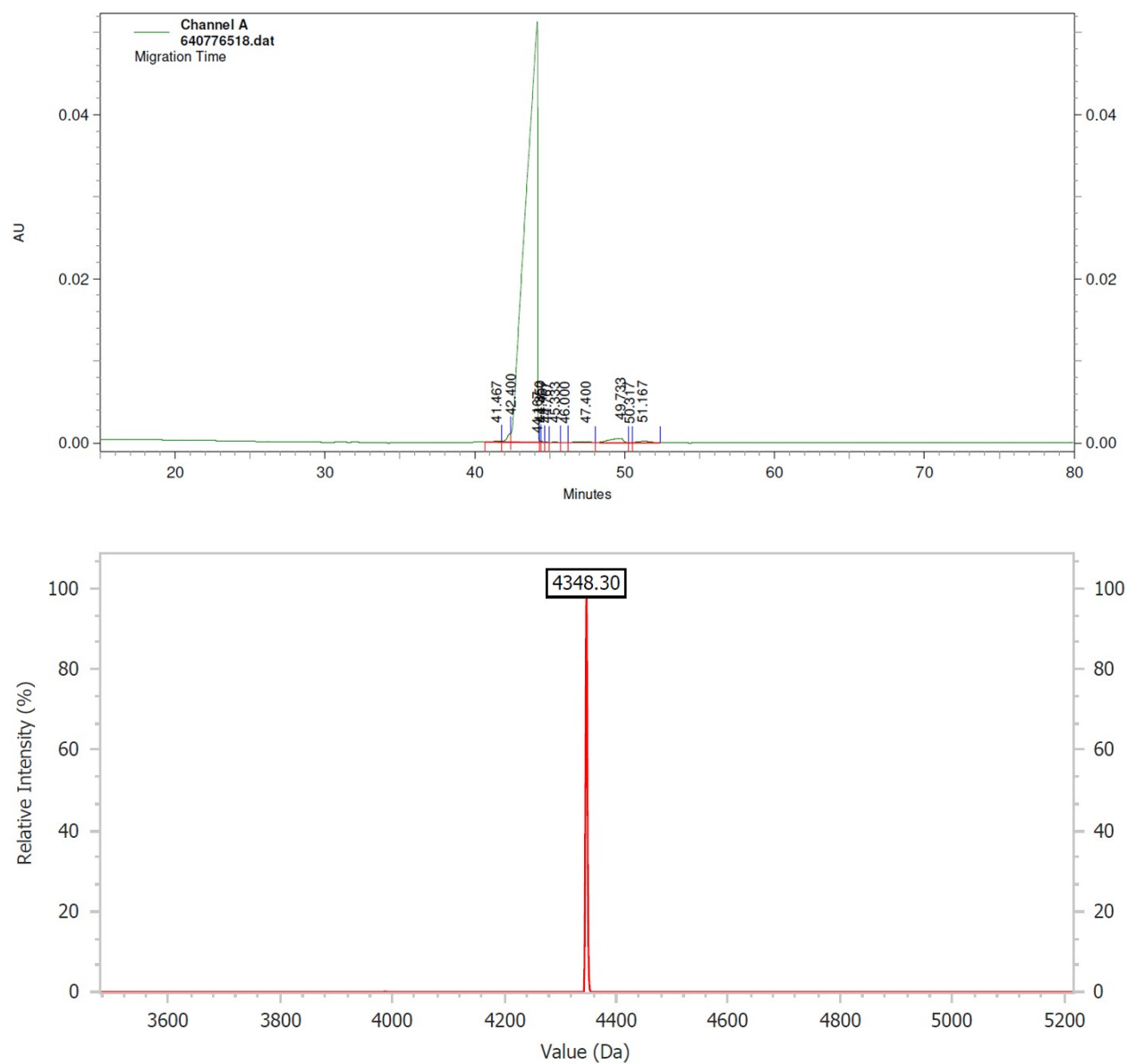
Figure S15. Capillary electrophoresis electropherogram (top) and ESI-MS spectrum (bottom) for **fullOMe**. Data provided by IDT.
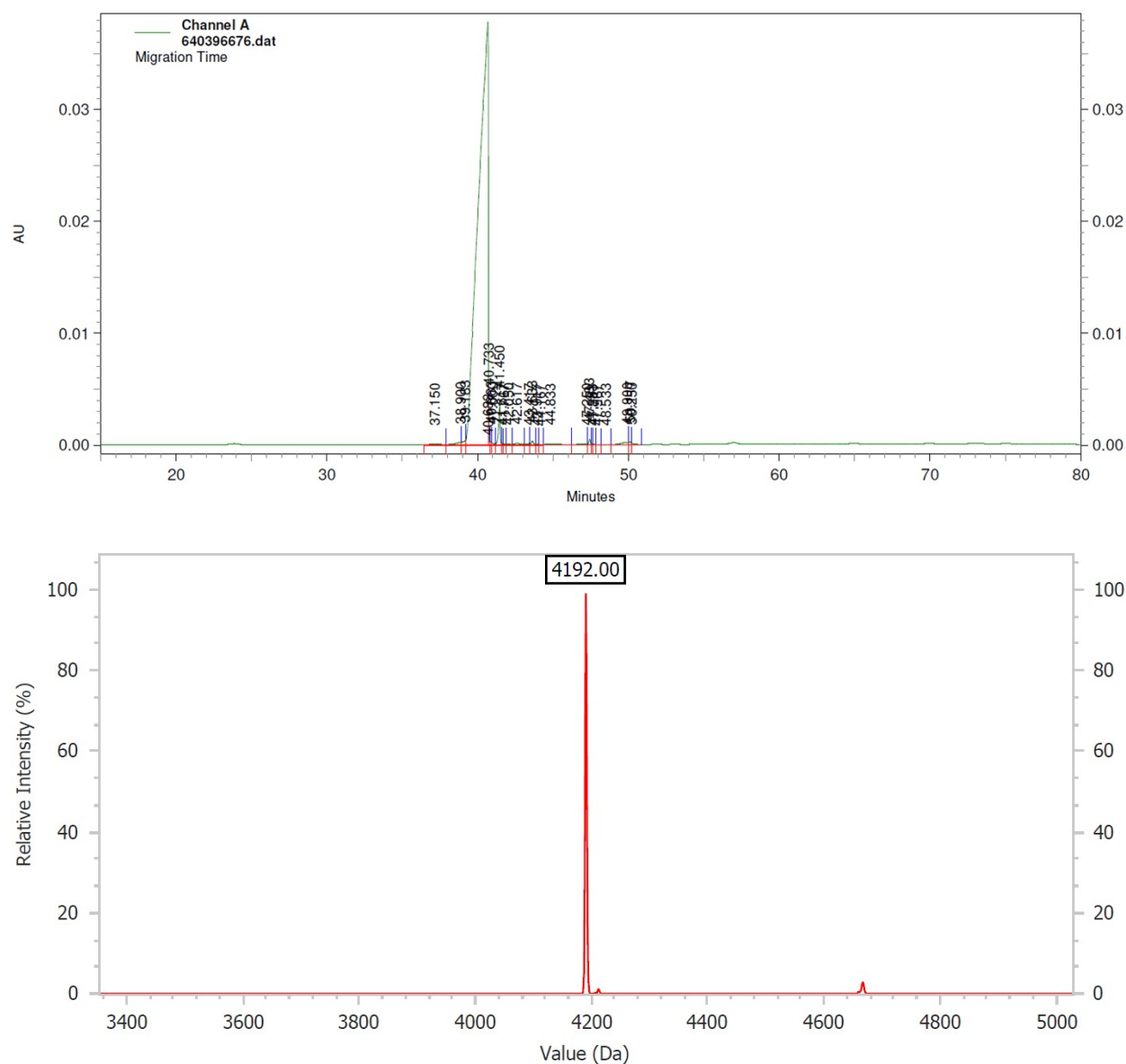
Figure S16. Capillary electrophoresis electropherogram (top) and ESI-MS spectrum (bottom) for **fullF**. Data provided by IDT.

SUPPLEMENTARY REFERENCES

S1.   R. Emehiser, E. Hall, D. C. Guenther, S. Karmakar and P. J. Hrdlicka, *Org. Biomol. Chem.*, 2020, **18**, 56–65.

S2.   M. E. Everly, R. G. Emehiser and P. J. Hrdlicka, *Org. Biomol. Chem.*, 2025, **23**, 619–628.

S3.   N. N. Dioubankova, A. D. Malakhov, D. A. Stetsenko, M. J. Gait, P. E. Volynsky, R. G. Efremov and V. A. Korshun, *ChemBioChem*, 2003, **4**, 841–847.

S4.   J. L. Mergny and L. Lacroix, *Oligonucleotides*, 2003, **13**, 515537.

S5.   M. E. Everly, P. J. Wieber, I. Al Janabi and P. J. Hrdlicka, An electrophoretic mobility shift assay with chemiluminescent readout to evaluate DNA-targeting oligonucleotide-based probes, *protocols.io*, 2025, DOI: 10.17504/protocols.io.4r3l218rxg1y/v1.

S6.   M. E. Everly, MeEverly/DNA-Invasion-Protocol: Release for DR_Script (v1.0.1). *Zenodo*, 2025, DOI: 10.5281/zenodo.15579929.

S7.   M. E. Everly, MeEverly/Oligo-Data: Oligo-Data-Visualization-With-R (v1.0.0), *Zenodo*, 2025, DOI: 10.5281/zenodo.15660406.

S8.   L. D. Williams, M. Egli, Q. Gao and A. Rich, DNA intercalation: Helix unwinding and neighbor-exclusion. In Structure and Function: Nucleic Acids; R. H. Sarma and M. H. Sarma, Eds.; Adenine Press: Albany, NY, USA, 1992; Volume 1, pp. 107–125.

S9.   H. Ihmels and D. Otto, *Top. Curr. Chem.*, 2005, **258**, 161–204.

S10.   O. Persil and N. V. Hud, *Trends Biotechnol*. 2007, **25**, 433–436.

S11.   S. C. Jain, C. Tsai and H. M. Sobell, *J. Mol. Biol*. 1977, **114**, 317–331.

S12.   S. P. Sau, A. S. Madsen, P. Podbevsek, N. K. Andersen, T. S. Kumar, S. Andersen, R. L. Rathje, B. A. Anderson, D. C. Guenther, S. Karmakar, P. Kumar, J. Plavec, J. Wengel and P. J. Hrdlicka, *J. Org. Chem*. 2013, **78**, 9560–9570.

S13.   S. Karmakar, A. S. Madsen, D. C. Guenther, B. C. Gibbons and P. J. Hrdlicka, *Org. Biomol. Chem*., 2014, **12**, 7758–7773.

S14.   H. Asanuma, T. Fujii, T. Kato and H. Kashida, *J. Photochem. Photobiol., C*, 2012, **13**, 124135.

S15.   R. Emehiser and P. J. Hrdlicka, *Org. Biomol. Chem.*, 2020, **18**, 1359–1369.

S16.   D. C. Guenther, G. H. Anderson, S. Karmakar, B. A. Anderson, B. A. Didion, W. Guo, J. P. Verstegen and P. J. Hrdlicka, Chem. Sci., 2015, 6, 5006–5015.